

Paper 13-3 has been designated as a Distinguished Paper at Display Week 2018. The full-length version of this paper appears in a Special Section of the *Journal of the Society for Information Display (JSID)* devoted to Display Week 2018 Distinguished Papers. This Special Section will be freely accessible until December 31, 2018 via:

http://onlinelibrary.wiley.com/page/journal/19383657/homepage/display_week_2018.htm

Authors that wish to refer to this work are advised to cite the full-length version by referring to its DOI:

<https://doi.org/10.1002/jsid.634>

Highly Efficient Deep-Blue Fluorescent Dopant for Achieving Low-Power OLED Display Satisfying BT.2020 Chromaticity

Yusuke Takita, Naoaki Hashimoto, Kyoko Takeda, Shiho Nomura, Shogo Uesaka, Tsunenori Suzuki, Harue Nakashima, Satoshi Seo, and Shunpei Yamazaki
Semiconductor Energy Laboratory Co., Ltd., Kanagawa, Japan

Abstract

We have succeeded in developing a stable deep-blue fluorescent dopant which has a shorter emission wavelength and higher emission efficiency than conventional pyrene-based dopants. It was revealed that the power consumption of a panel using this novel dopant was estimated to be lower than that of a conventional one.

Author Keywords

OLED; Fluorescent OLED; Deep Blue; BT.2020 color gamut

1. Introduction

Organic light-emitting diodes (OLEDs) have been actively researched for application to various light-emitting devices including displays, ever since a high efficiency device with a heterostructure was reported in 1987 [1]. Considering the application to active matrix OLEDs (AMOLEDs), firstly it is important to develop backplanes, i.e. FETs, suitable for the OLEDs. Previously, we have discovered new crystal structures different from single crystal In-Ga-Zn oxide (IGZO) and amorphous IGZO, namely CAAC IGZO and nanocrystal IGZO [2–5], and have reported AMOLEDs using these as backplanes [6–8]. In terms of the performance of the OLEDs, improving the efficiency and the color gamut of blue devices are important challenges. Recently, the BT.2020 color gamut has been proposed as a standard for 8K displays [9]. A deeper-blue light-emitting material with a shorter wavelength compared with conventional materials is necessary to cover this color gamut.

It is well-known that the efficiency of blue-fluorescent devices can be increased by utilizing triplet-triplet annihilation (TTA) [10, 11]. Previously, we demonstrated a stable blue-fluorescent device with a high efficiency based on TTA [12–14]. The external quantum efficiency (EQE) of a device with a fluorescent dopant with a conventional pyrene skeleton can reach approximately 13% at the maximum, which is high compared with the typical EQEs of fluorescent devices. However, the EQE of the device tends to become low as chromaticity is improved. We reported BD-02 as a fluorescent dopant that exhibits BT.2020 blue light ($x = 0.131$, $y = 0.046$). However, the EQE of the device with BD-02 is only approximately 10% [15]. This low EQE is attributed to (1) the low photoluminescence quantum yield (PLQY) of the dopant and (2) a decrease in the efficiency of energy transfer from a host resulting from the short absorption wavelength of the dopant.

In this study, we developed novel dopants with heteroaromatic ring skeletons different from a pyrene skeleton. Compared with BD-02, a conventional pyrene-based deep-blue dopant, the new dopants generate a deeper blue and have higher efficiency. Moreover, we successfully achieved the BT.2020 blue color by incorporating a microcavity structure. The power consumption of a display using the novel dopant was estimated to be low compared with a display using the conventional dopant.

2. Novel deep-blue dopant

First, the emission characteristics of the new dopants were compared with those of BD-02. Figure 1 compares the photoluminescence (PL) spectra of our blue dopants, BD-02, BD-05, and BD-06 in toluene solutions. BD-02 has a peak at 450 nm, indicating that an OLED device containing BD-02 along with a microcavity structure satisfies BT.2020 blue emission. The EQE of this OLED, however, is not high enough, even though TTA mechanism is assumed to contribute to the increase of EQE. We developed two dopants, BD-05 and BD-06, each with a heteroaromatic ring skeleton different from a pyrene skeleton. The two dopants have the same skeletal luminophore but show some differences in PL spectra. Change of a substituent attached to the heteroaromatic skeleton is effective for the shift of PL spectra. The PL spectra of BD-05 and BD-02 have peaks at similar locations (448 and 450 nm, respectively), while the peak in the spectrum of BD-06 is located at a shorter wavelength (441 nm). It should be also noted that the shoulder peaks of BD-05 and BD-06 are less intense than that of BD-02, and the main peaks of the novel dopants are sharper than that of BD-02. These spectral features indicate that the novel materials should be effective for obtaining deep-blue light emission when used in devices with microcavity structures.

Table 1 shows the PL quantum yields (PLQYs) of the dopants in toluene solutions. The PLQY of BD-02 was 91%, whereas those of BD-05 and BD-06 were 93% and 97%, respectively, and higher than that of BD-02. This indicates that BD-05 and BD-06 are excellent blue dopants with high PLQYs, in addition to sharper spectra at shorter peak wavelength.

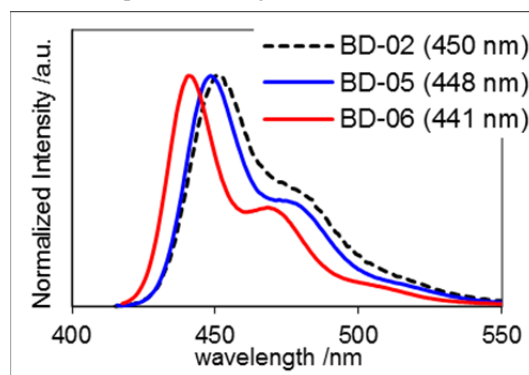


Figure 1 Photoluminescence (PL) spectra of BD-02, BD-05, and BD-06 in toluene solutions (values of peaks are shown in parentheses).

Table 1 Photoluminescence quantum yield (PLQY) of BD-02, BD-05, and BD-06 in toluene solutions.

	BD-02	BD-05	BD-06
PLQY / %	91	93	97

3. Device characteristics

Bottom-emission devices (Devices 5 and 6) were fabricated using BD-05 and BD-06, respectively. Device 2 using BD-02 was also fabricated for reference. The device structures are shown in Fig. 2. Figures 3 and 4 compare the electroluminescence (EL) spectra and EQEs of three devices, respectively. The EL spectrum of Device 5 has a peak at 457 nm, which substantially overlaps with that of Device 2. The EL peak of Device 6 locates at a shorter wavelength (451 nm) than that of Device 2. It should be noted that the emission wavelengths of Devices 5 and 6 using our novel dopants are short enough to satisfy the chromaticity coordinates of the BT.2020 blue color, when an optimized microcavity structure is incorporated into the devices. The EQEs of Devices 5 and 6 at approximately 1,000 cd/m² are 11.8% and 11.4%, respectively, and higher than that of Device 2 (10.7%). As is shown in Table 1, the PLQYs of BD-05 and BD-06 are little bit higher than that of BD-02. This small difference in PLQY, however, does not give

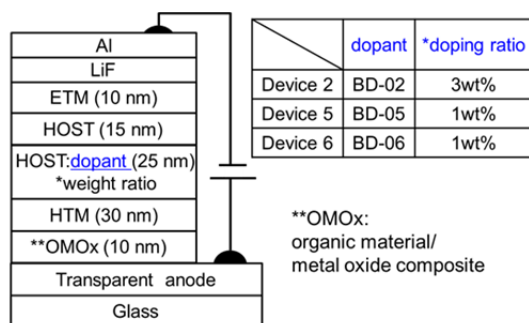


Figure 2 Structures of Devices 2, 5, and 6.

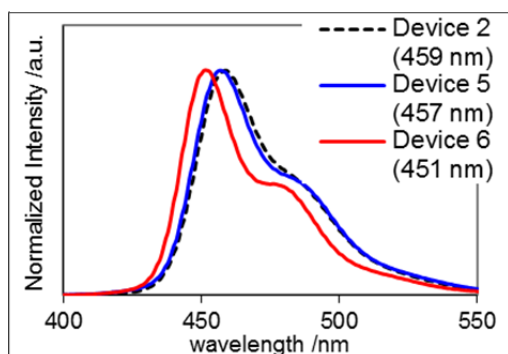


Figure 3 Electroluminescence (EL) spectra of Devices 2, 5, and 6 (values of peaks are shown in parentheses).

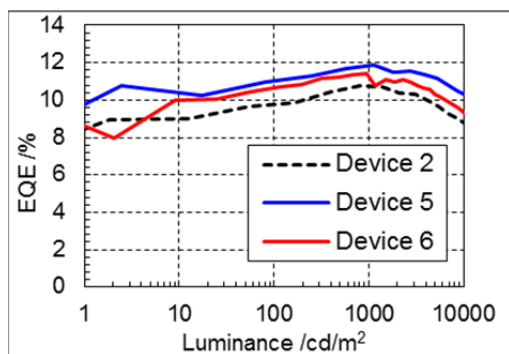


Figure 4 External quantum efficiencies (EQEs) of Devices 2, 5 and 6.

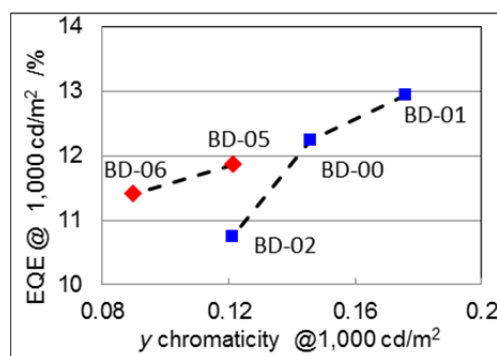


Figure 5 Correlations between y chromaticity and EQE for devices based on conventional pyrene-based dopants (BD-00, BD-01, and BD-02) and novel dopants with heteroaromatic ring skeletons (BD-05 and BD-06).

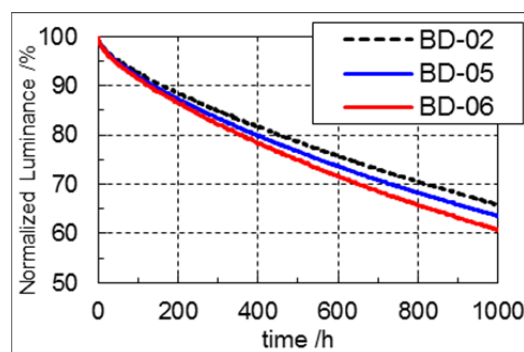


Figure 6 Normalized luminance decay curves of Devices 2, 5, and 6 driven at a constant current density (50 mA/cm²).

reason for the large difference in EQE between devices (in particular, between Devices 2 and 5). We assume that the efficiency of energy transfer from singlet excitons of host molecules to those of guest molecules may be the major origin of the difference of EQEs. In other words, the high EQEs of Devices 5 and 6 are explained by higher efficiency of energy transfer from the host to BD-05 and BD-06 than that from the host to BD-02. The details are described in section 4.

Figure 5 shows the correlations between the y chromaticity and EQE of the bottom-emission devices fabricated using the different dopants. In Fig. 5, the data of dopants (BD-00 and BD-01), each of which has the same pyrene skeleton as that of BD-02 and emits light with a longer wavelength than that of BD-02, are added. As the y chromaticity improved, the EQEs of the devices based on BD-00, BD-01, and BD-02, which are conventional pyrene-based dopants, decreased significantly, and the EQE of the deep-blue dopant BD-02 dropped down to less than 11%. In contrast, BD-05 and BD-06 retained high efficiency, even when y chromaticity shifted to deep blue.

Figure 6 shows the normalized luminance decay curves of the devices driven at a constant current density (50 mA/cm²). The 10% luminance decay time (LT90) values of Devices 5 and 6 were 140 and 125 h, respectively. These LT90 values are nearly comparable with that of Device 2 (150 h).

Table 2 lists the major device characteristics at approximately 1000 cd/m². Devices based on BD-05 and BD-06 demonstrated high efficiency, while the chromaticity of BD-05 was essentially

equal to that of BD-02, whereas the chromaticity of BD-06 was better than that of BD-02. It is worth emphasizing that three major requirements, deep-blue chromaticity, high efficiency, and high durability are all satisfied in Devices 5 and 6 using our novel dopants, BD-05 and BD-06.

Table 2 Device characteristics of Devices 2, 5, and 6 at approximately 1,000 cd/m².

	Voltage (V)	Current Density (mA/cm ²)	Chromaticity		Current Efficiency (cd/A)	EQE(%)	LT90 (h) [50 mA/cm ²]
			x	y			
Device 2	3.10	7.77	0.140	0.121	10.4	10.7	150
Device 5	3.10	9.60	0.140	0.122	11.6	11.8	140
Device 6	3.10	10.2	0.141	0.090	9.15	11.4	125

4. Energy transfer from host to dopant

In this section, the factor contributing to the higher efficiencies of Devices 5 and 6 relative to that of Device 2 is considered in terms of energy transfer from the host to the dopant. Considering the energy transfer from a host to a dopant via the Förster mechanism, the efficiency of the energy transfer increases with increasing overlap between the emission spectrum of the host and the molar-absorptivity spectrum of the dopant [16].

Figure 7 shows the PL spectrum of the host (a 50-nm-thick thin film) and the absorption spectrum of each dopant in a toluene solution (the vertical axis represents the molar absorption coefficient). The PL spectrum of the host is in arbitrary scale, but the vertical axis of the absorption spectra of the dopants is scaled by a molar absorption coefficient (M⁻¹cm⁻¹).

Although the emission wavelength of BD-05 is substantially the same as that of BD-02 as shown in Fig. 1, marked difference between the absorption spectra of BD-02 and BD-05 was found. BD-05 has an absorption peak at a longer wavelength than that of BD-02 and has a higher molar absorption coefficient than BD-02. Thus, the overlap between the emission spectrum of the host and the absorption spectrum of BD-05 is larger than the overlap between the emission spectrum of the host and the absorption spectrum of BD-02. This difference in overlap implies that the rate of energy transfer from the host to BD-05 is higher than that to BD-02, resulting in a higher EQE of BD-05 than that of BD-02.

By contrast, the peak wavelength in the absorption spectrum of BD-06 is substantially the same as that of BD-02, whereas the molar absorption coefficient of BD-06 is much larger than that of

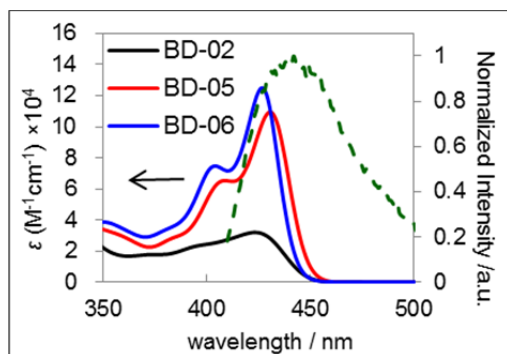


Figure 7 An overlap between a PL spectrum (broken curve) of a host (thin film) and an absorption spectrum (solid curve) of each dopant in a toluene solution. The PL spectrum of the host is in arbitrary scale, and the vertical axis is scaled by a molar absorption coefficient ϵ (M⁻¹cm⁻¹) of the absorption spectrum of the dopant.

BD-02. Therefore, it is assumed that the rate of energy transfer from the host to BD-06 is higher than that to BD-02 but lower than that to BD-05. This order of the rate of the energy transfer, we examined here, well corresponds to the EQE of the devices, and this facts gives a rationale for the influence of the rate of energy transfer on EQE in our dopant/host system.

5. Device optimization for OLED displays satisfying BT.2020 standard

Top-emission devices with microcavity structure were fabricated to obtain blue light satisfying the BT.2020 standard. The microcavity structure increases the intensity of light of a specific wavelength and allows the light to be extracted via the optical resonance effect between electrodes. Top-emission devices based on essentially the same device structure with the bottom-emission devices were fabricated. In these devices, the thicknesses of HILs (OMOX; organic material/metal oxide composite) were varied to change the optical resonance wavelength. Note that OMOx, which is a HIL we developed originally, is a mixed layer of a hole-transport material and molybdenum oxide (MoO₃) [17]. Because our original OMOx shows no absorption in the visible region [14], the emission efficiency is not influenced by the film thickness of HIL, even when the thickness of the OMOx layer is changed for optimizing microcavity structures. A 10-nm mixed film of Ag and Mg (weight ratio: 1:0.1) was used as a semitransparent cathode.

The relationships between y chromaticity and current efficiency of the devices using the three dopants were investigated. Figure 8 shows the relationships between y chromaticity and current efficiency at approximately 1000 cd/m². In the region of pure-blue chromaticity according to the NTSC standard ($y = 0.08$) or the sRGB standard ($y = 0.06$), the device based on BD-05 had a higher current efficiency than the device based on BD-02. This is primarily because the efficiency of energy transfer from the host to BD-05 is higher than that to BD-02. On the other hand, as the y chromaticity improved, the difference in current efficiency between the devices based on BD-06 and BD-02 increased. For the blue chromaticity of the BT.2020 standard ($y = 0.046$), the current efficiency of the device based on BD-06 is approximately 1.7 times higher than that of the device based on BD-02. This difference is primarily attributed to shorter emission wavelength of BD-06 than that of BD-02. Thus, it is concluded that BD-06, which has a shorter emission wavelength than BD-02, has advantage for achieving the emission of light with BT.2020

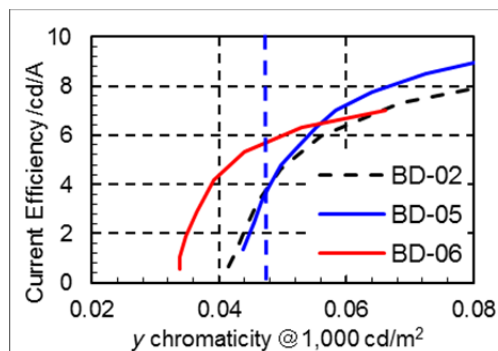


Figure 8 Relationships between y chromaticity and current efficiency when microcavity structure is used in top-emission devices based on BD-02, BD-05 and BD-06 (the blue broken line in graph shows y chromaticity of BT.2020 standard [$y = 0.046$]).

deep-blue chromaticity. Accordingly, BD-05 is an effective dopant for producing the pure-blue chromaticity of the NTSC standard or the sRGB standard, and BD-06 is an effective dopant for the deep-blue chromaticity of the BT.2020 standard.

Next, we estimated the power consumption of panels by assuming the case when OLED panels are fabricated by side-by-side patterning. We assumed the use of our green and red light-emitting materials satisfying the BT.2020 standard, on which we reported previously, for green and red pixels [18, 19]. Then, two OLED panels, referring to panel B2 and panel B6, using BD-02 and BD-06 for a blue pixel, respectively, were examined. Tables 3 show the power consumptions of the panels assumed to display D65 white (CIE(x, y) = 0.313, 0.329) over the entire screen (with a size of 4.3 inches and an aspect ratio of 16:9) at a luminance of 300 cd/m² with the aperture ratio of the panel of 15%

Table 3 Estimated characteristics of top-emission panels fabricated by side-by-side patterning using BD-02 and BD-06 when the panels emit D65 white light at 300 cd/m².

		Panel B2		Panel B6	
Chromaticity	R	0.713	0.287	0.713	0.287
	G	0.182	0.786	0.182	0.786
	B	0.145	0.046	0.146	0.045
BT.2020 area ratio (CIE(u',v'))(%)		101		101	
Panel luminance (cd/m ²)	R	73		72	
	G	209		210	
	B	18		18	
Pixel luminance (cd/m ²)	R	3631		3623	
	G	10470		10497	
	B	899		879	
Voltage (V)	R	4.0		4.0	
	G	3.4		3.4	
	B	3.2		3.1	
Current efficiency (cd/A)	R	36.5		36.6	
	G	95.3		95.3	
	B	3.2		5.5	
Power consumption (mW/cm ²)		8.3		6.3	

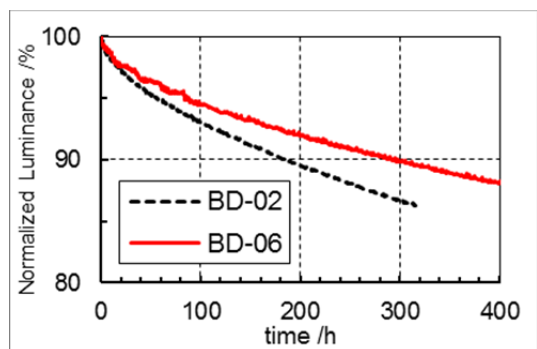


Figure 9 Normalized luminance decay curves of top-emission devices with BD-02 and BD-06 when driving at the pixel luminance estimated in Table 3. Each driving current density is 25.8 mA/cm² for the device with BD-02 and 15.8 mA/cm² for the device with BD-06.

[5% each for the red, green, and blue (R, G, and B, respectively) subpixels] and light attenuation (e.g., resulting from a circularly polarizing plate) of 60%. The panel luminance of each color (R, G, and B) corresponds to the luminance of the corresponding color component necessary to obtain D65 white color with a luminance of 300 cd/m². Pixel luminance refers to the intrinsic luminance of a subpixel. The BT.2020 area ratio of each panel is larger than 100%. It should be noted that the power consumption of the whole panel B6 (6.3 mW/cm²) was 24% smaller than that of the whole panel B2 (8.3 mW/cm²). As one finds out from y chromaticity vs. current efficiency relationship in Fig. 8, the low-power consumption of the panel B6 is attributed to the improved current efficiency at the chromaticity close to the BT.2020 chromaticity due to the use of BD-06.

Lastly, the reliabilities of the dopants at the pixel luminances estimated in Table 3 were compared. Figure 9 shows the normalized luminance decay curves of top-emission devices with BD-02 and BD-06. The device with BD-06 exhibited less deterioration than the device with BD-02. This marked improvement in reliability is originated from the fact that the efficiency of the device using BD-06 was substantially improved, and thus, its current density at the pixel luminance was reduced.

6. Summary

We developed two types of blue-fluorescent dopants, each with a novel heteroaromatic ring as the skeleton. The EQEs of the bottom-emission devices fabricated using the novel dopants were approximately 1.1 times higher than that of the device based on a conventional pyrene-based dopant, while the lifetimes were comparable. Moreover, the current efficiencies of devices with a microcavity structure based on the novel dopants at chromaticity close to the BT.2020 standard are approximately 1.7 times higher than those of the device based on the conventional dopant. As a result, the power consumption of OLED panels fabricated by RGB side-by-side patterning using the novel dopants were estimated to be lower than that of the panel fabricated using the conventional dopant.

References

- [1] C. W. Tang *et al.*, *Appl. Phys. Lett* **51**, 913 (1987)
- [2] S. Yamazaki *et al.*, *SID Symposium Digest* **43**, 183(2012)
- [3] S. Yamazaki *et al.*, *Jpn. J. Appl. Phys* **53**, 04ED18 (2014)
- [4] S. Ito, *et al.*, AM-FPD'13, Dig. 151-154 (2013).
- [5] S. Yamazaki & N. Kimizuka, *Physics and Technology of Crystalline Oxide Semiconductor CAAC-IGZO: Fundamentals*, (Wiley Series in Display Technology, 2016)
- [6] A.Chida *et al.*, *SID Symposium Digest* **44**, 196 (2013)
- [7] S. Kawashima *et al.*, *SID Symposium Digest* **45**, 627 (2014)
- [8] M. Shiokawa *et al.*, *SID Digest* **47**, 1209 (2016)
- [9] ITU-R Recommendation BT.2020-2 (2015).
- [10] D. Y. Kondakov *et al.*, *J. Appl. Phys.* **106**, 124510 (2009)
- [11] D. Y. Kondakov, *J. Appl. Phys.* **102**, 114504 (2007)
- [12] N. Hashimoto *et al.*, *SID Symposium Digest* **47**, 301 (2016).
- [13] T. Suzuki *et al.*, *Jpn. J. Appl. Phys.* **53**, 052102 (2014)
- [14] S. Yamazaki & T. Tsutsui, *Physics and technology of Crystalline oxide semiconductor CAAC-IGZO: application to display* (Wiley Series in Display technology, 2017)
- [15] N. Hashimoto *et al.*, *SID Symposium Digest* **48**, 786 (2017)
- [16] T. Förster, *Ann. Phys.* **2**, 55 (1948)
- [17] H. Ikeda *et al.*, *SID Symposium Digest* **37**, 923 (2006)
- [18] S. Hosoumi *et al.*, *SID Symposium Digest* **48**, 13 (2017)
- [19] T. Sasaki *et al.*, *SID Symposium Digest* **48**, 123 (2017)